Photocatalytic properties of ZnO thin film with different morphologies from seed, array to grass

Zhaopeng Wang[1], *Xiaoyun Ye*[1,2,3,4] ✉, *Long Chen*[1], *Leilei Zhang*[1], *Qianting Wang*[1,2,3,4], *Lian Ma*[1,2,3,4], *Nengbin Hua*[1,2,3,4]

[1]*School of Materials Science and Engineering, Fujian University of Technology, Fuzhou 350118, People's Republic of China*
[2]*Fujian Provincial Key Laboratory of Advanced Materials Processing and Application, Fuzhou 350118, People's Republic of China*
[3]*Mould Technology Development Base of Fujian Province, 33 South Xuefu Road, Fuzhou 350118, People's Republic of China*
[4]*Fuzhou Innovation Platform for Novel Materials and Mould Technology, 33 South Xuefu Road, Fuzhou 350118, People's Republic of China*
✉ *E-mail: creekye@163.com*

Published in Micro & Nano Letters; Received on 21st January 2020; Revised on 17th February 2020; Accepted on 21st February 2020

ZnO thin film with different morphologies from seed, array to grass was grown by simple aqueous solution method under room temperature. The morphologies, structure, optical properties and photocatalytic properties of the samples were characterised by transmission electron microscope, scanning electron microscope, X-ray diffraction, fluorescence spectrometer, UV–Vis spectrophotometer and photocurrent response. The results showed that the ZnO arrays and grassy ZnO were both hexagonal wurtzite with uniform distribution and regular growth on the glass substrate. ZnO thin film with different morphologies affected the utilisation efficiency of the ultraviolet light. Multiple light reflections inside the grassy ZnO greatly increase the light efficiency. The methyl blue degradation rate of grassy ZnO photocatalyst was superior under the UV light compared to the other ZnO morphologies. Grassy ZnO showed favourable stability after five cycles. The comparison of the ZnO semiconductor in different dimensions is helpful for further research on other photocatalysts as well as their potential application.

1. Introduction: In the recent years, the environmental issues have been widely concerned. Environmental pollution includes air pollution, soil pollution and water issues [1–3]. The water issues have been on the focus of increasing international concern, especially the treatment of harmful organic dyes, which has become one of the most important issues in water pollution [4]. So far, there are many ways to treat organic dyes; photocatalysis is one of the technologies studied in depth [5]. It can be shown that many semiconductor metal oxides [6] have been chosen to investigate the photocatalytic degradation performance of dyes, including TiO_2 [7], ZnO [8], ZrO_2 [9], WO_3 [10] and so forth.

ZnO with the wide bandgap equivalent to TiO_2 (ca. 3.2 eV) [11] and unique high exciton binding energy of 60 meV has been used as a highlight material for photocatalytic applications on account of its physical and chemical application [12, 13]. ZnO with different morphologies and latitude [14, 15] plays an important role in photocatalysis field. Liu *et al.* [16] synthesised ZnO nanowires by electrostatic spinning method to degrade methyl blue (MB) solution under ultraviolet light with the best degradation efficiency of 50% after 360 min. Li *et al.* [17] reported that the degradation rate of ZnO nanorod reached 20% after 120 min in the RhB solution under sunlight. The flake-like ZnO fabricated by Wu *et al.* [18] was utilised to photo-degrade Brilliant Red X-3b aqueous solution at the wavelength of 365 nm and showed certain degradability. Mauro *et al.* [19] investigated the photocatalytic degradation of MB solution by ZnO films with different thickness under ultraviolet light, but the degradation rate of that was only 50% after 240 min. Numerous examples show that ZnO has relatively acute photocatalytic response. However, the above data reveal that the photocatalytic properties of the ZnO materials should be improved and further studied. It is noticed that most of the ZnO catalysts are powdered. It is troublesome to recycle in the testing process. In contrast, ZnO film is relatively advantageous and can achieve the same performance [20]. Furthermore, there is little comparison between ZnO in different dimensions.

In this Letter, ZnO with different morphologies were grown on the glass substrate by *in-situ* growth method to form photocatalyst. The effect on organic dyes MB under UV light was investigated. The structure, morphology and photocatalytic properties of ZnO seed layers, ZnO arrays and grassy ZnO photocatalysts were studied. The grassy ZnO with excellent performance is expected to be widely concerned in the field of photocatalysis and applied in practice.

2. Experimental section

2.1. Materials: Zinc acetate ($Zn(CH_3COO)_2$), hexamethylenetetramine (HMTA), sodium hydroxide (NaOH), polyethyleneimine (PEI, Mw1800), ammonia ($NH_3{\cdot}H_2O$, 25–27%), absolute ethanol (C_2H_5OH), sodium sulphate (Na_2SO_4) and zinc nitrate ($Zn(NO_3)_2{\cdot}6H_2O$) were purchased from Sinopharm Chemical Reagent Co., Ltd. All compounds were prepared using analytical grades.

2.2. Preparation of the ZnO seed layer: Concretely, 25 ml of zinc acetate (0.02 M) ethanol solution was stirred for 30 min at 58°C, 25 ml of sodium hydroxide (0.03 M) ethanol solution was stirred for 30 min at room temperature and then added into the above solution. The solution was agitated vigorously for 120 min to obtain the seeds solution. The seeding process was carried out by spinning coatings onto the glass substrate with seeds solution at 3000 rpm for 20 s. This operation was repeated six times. The seed layer was annealed at 400°C for 1 h [21].

2.3. Growth of the ZnO arrays: The seeded substrate was diagonally placed into the mixture of the aqueous solution of zinc nitrate and hexamethylenetetramine with equal molar concentrations (0.05 M) ($v/v = 4{:}1$) were preheated in an oven at 80°C for 30 min then placed at 80°C for 24 h. Subsequently, the substrate was washed by deionised water and dried in air. The final substrate was placed in a 400°C resistance oven for 1 h.

doi: 10.1049/mnl.2020.0017

2.4. Growth of the grassy ZnO: The seed-layer substrate was also introduced to prepare the grassy ZnO as the contrast test. The substrate was diagonally placed into a mixture with 0.05 M of zinc nitrate aqueous solution, 0.05 M of hexamethylenetetramine, 5 mM of polyethyleneimine and a certain amount of ammonia (0.35 and 0.65 M), and heated in an oven at 83°C for 1.5 h, and 90°C for another 1 h. Subsequently, the substrate was washed by deionised water and ethanol absolute whereafter dried in air. The substrate was annealed in 450°C for 0.5 h. The corresponding samples were named to Grass-1 and Grass-2 for the different amount of ammonia (0.35 and 0.65 M), respectively. The ZnO with different morphologies were shown in Fig. 1.

2.5. Characterisation: The sample will be characterised by structural, optical and photocatalytic activity. The sample structure was mainly tested by an X-ray diffractometer (XRD, D8-ADVANCE, BRUKER, Germany) with $2\theta = 10–80°$. The sample absorption spectrum was tested by UV–Vis spectroscopy (UV 2600, PerkinElmer, USA) with a test wavelength of 200–800 nm. The surface topography of the sample was observed using a field emission scanning electron microscope (NANONOVASEM 450, FEI, USA). The microstructure and distribution of ingredient for the samples were demonstrated by transmission electron microscopy (TEM, G2 F20, FEI, USA) with an energy disperse spectroscopy. A Fourier infrared spectroscopy analyser (FTIR, Nicolet 6700, Thermo, USA) was used to confirm the sample structure. A steady-state fluorescence spectrometer (FLS980, Eindhoven, Germany) was used to test samples using a Xenon lamp with a test excitation wavelength of 325 nm. The Xenon lamp source system (CEL-HXF 300, Beijing Zhongjiao) was used to drive the photocatalytic experiment with a 200–420 nm lamp source.

2.6. Photocatalytic activity: The photocatalytic activities of the samples were estimated through the decomposition of MB under UV irradiation at room temperature. Typically, the substrate of photocatalyst was absolutely immersed in aqueous solution of MB dye (10 mg/l, 60 ml). The substrate was placed in homemade frame and stirred in the dark for 30 min and then treated by a 300 W Xenon arc lamp as light source. For a 15 min interval, a certain amount of solution (~5 ml) was taken out. Subsequently, the concentration of MB in supernatant liquid was measured from the maximum absorption ($\lambda = 665$ nm) by a UV–Vis spectrophotometer. The photocurrent densities were performed on a CHI660E electrochemical workstation with a 300 W Xenon full-band source.

FTO (1 cm × 3 cm) pieces were grown with ZnO photocatalysts as photoanode. Pt acted as counter electrode and Ag/AgCl served as reference electrode in the reaction. Na_2SO_4 (0.5 M) was selected as test electrolyte.

3. Results and discussion

3.1. Morphology analysis: Fig. 2 shows TEM and HRTEM images of the ZnO nanoparticles for forming a seed layer and ZnO nanorod to build a ZnO three-dimension structure, respectively. In Fig. 2*a*, spherical grains of uniform size (~8 nm) in diameter with a clear outline and good dispersion are shown. The high-resolution TEM image (Fig. 2*b*) displays the interplanar spacing of 0.253 nm, which corresponds to the (002) crystal plane of wurtzite ZnO.

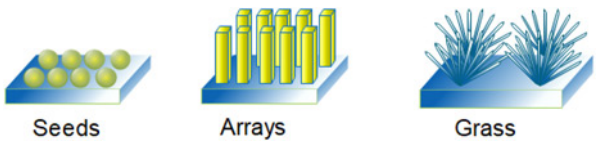

Fig. 1 *Schematic diagram of ZnO with different morphologies*

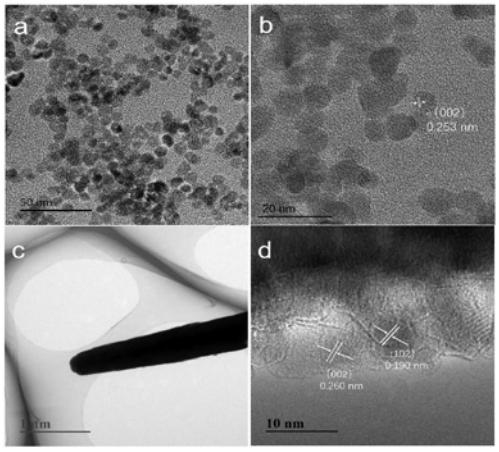

Fig. 2 *TEM and HRTEM of the samples*
a TEM of ZnO particles
b HRTEM of ZnO particles
c TEM of grassy ZnO
d HRTEM of grassy ZnO

Single ZnO nanorod (Figs. 2*c* and *d*) also presents good crystallinity with the interplanar spacing of 0.19 and 0.26 nm, which are assigned to the (102) and (002) crystal planes of wurtzite ZnO.

To further investigate the growth of the ZnO on the substrate, the surface and the cross-section of the as-prepared samples were surveyed by scanning electron microscopy (SEM) (Fig. 3). It can be seen from Fig. 3*a* that seeds are evenly distributed on the surface of the glass substrate and form a dense ZnO film, which provides a seed layer to ensure the growth of the rod-like ZnO. In Fig. 3*b*, the ZnO arrays with dense ZnO nanorods exhibit the prospective geometry with hexagonal columns and good orientation to be perpendicular to the substrate. With the addition of PEI and ammonia, the shape of the ZnO changes from arrays to grass (Figs. 3*c* and *d*). It is obvious that the grass-like ZnO consists of the number of thin nanorods, where the ends are not hexagonal but show slightly pointed. Simultaneously, each ZnO nanorod that makes up the grass becomes thinner as the concentration of ammonia increases.

The increase of pH of the solution affects the aspect ratio of ZnO nanorods. It may be the reason that the variation of ammonia concentration regulates the concentration of zinc ions in the solution and leads to the change of ZnO growth. Even, the ZnO will be dissolved due to the high alkalinity from increased ammonia concentration [22].

In order to observe the growth of ZnO in detail, the cross-sections of ZnO nanorod arrays and ZnO grass are shown in Figs. 4*a* and *b*. It can be seen that ZnO array grows uniformly on the glass substrate

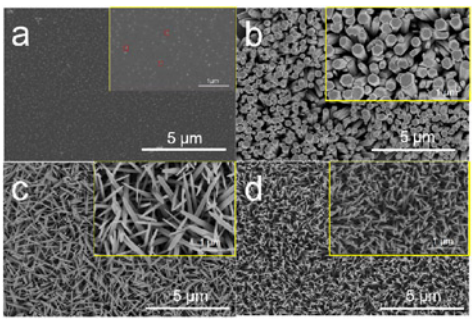

Fig. 3 *Scanning electron micrographs of the ZnO samples*
a Seeds
b Arrays
c Grass-1
d Grass-2

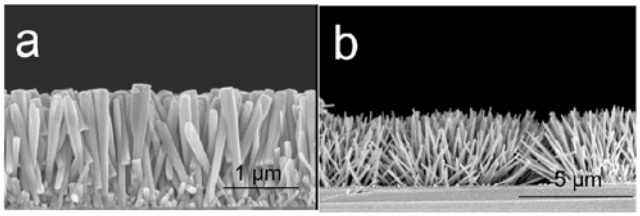

Fig. 4 *Sectional view of the samples*
a Arrays
b Grass-2

with a length of about 2 μm. The length of all the ZnO nanorods is consistent with good orientation. Moreover, a distinct grassy structure of ZnO with an average length of about 3 μm grown under alkaline conditions is presented. It can be speculated that the two samples grow along with *c*-axis perpendicular to the substrate with good crystallinity, which is consistent with HRTEM results. The selected element analysis of the grassy ZnO further demonstrated the typically main elements of Zn and O.

3.2. XRD analysis: For the observation of the crystalline ZnO with varied morphologies, XRD patterns were collected as shown in Fig. 5. All the ZnO samples exhibit typical diffraction peak at $2\theta = 31.8°$, 34.6°, 36.4°, 47.6°, 56.6°, 62.9°, 68.1° and 72.1°, which can be ascribed to (100), (002), (101), (102), (110), (103), (112) and (004) diffraction of hexagonal wurtzite ZnO (JCPDS Card No. 75-0576). The distinct higher intensity of (002) plane of the ZnO arrays and Grass-2 than that of Grass-1 indicates that the former two samples grow with *c*-axis of hexagonal wurtzite ZnO, which is consistent with the SEM results.

3.3. Photoluminescence (PL) analysis: The photo-physical properties of the ZnO nanostructures with different grown morphologies were further evaluated by PL spectra monitored at an excitation wavelength of 325 nm (Fig. 6). In all cases, the PL spectra show two distinct bands, one in UV region (near band emission) and another in visible region (defect emission band). The UV emission band is originated from the recombination of free exciton (electrons and holes) [23], while the broad visible emission band (>400 nm) is due to the inherent defects of oxygen vacancies and the impurities such as hydroxide and water [24]. These defects can trap the photo-induced electrons for reduction of the recombination of holes (h^+) and electrons (e^-) [25]. As can be seen from the spectra, the intensity of defect emission was found to be higher in the ZnO arrays and Grass than that of the ZnO seeds in the ultraviolet spectrum range. Simultaneously, the intensity of the defect peak increases from

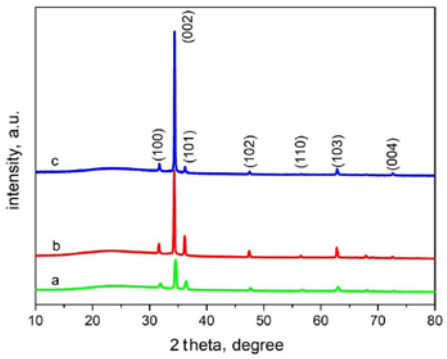

Fig. 5 *XRD curves of the samples*
a Grass-1
b Arrays
c Grass-2

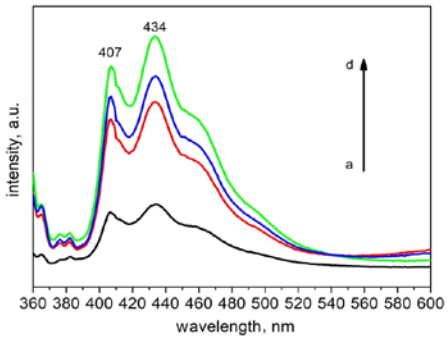

Fig. 6 *Fluorescence spectra of the samples*
a Seeds
b Arrays
c Grass-2
d Grass-1

arrays to grassy ZnO. The results clearly show that the defect emission band of the ZnO is strongly affected by the ZnO with different morphologies on the substrate under different conditions. On the other hand, more defects generated from grassy ZnO can effectively delay the recombination of the electron and hole. We thus assume that the photocatalytic performance of the grassy ZnO may be better than ZnO seeds and arrays, which will be further confirmed in the later part.

3.4. FTIR analysis: FTIR spectra of the ZnO with different latitudinal feature in the range of 400–4000 cm^{-1} were represented in Fig. 7. It can be clearly observed that strong O–H stretching at 3440 cm^{-1} corresponds to the presence of hydroxyl group on the surface of ZnO. Another peak at 1637 cm^{-1} is normally attributed to stretching vibration of hydroxyl groups from the adsorbed molecular water, indicating the presence of hydration in the samples [26]. In addition, other broad peak around 500 cm^{-1} is due to the symmetric stretching vibration mode of the Zn–O [27, 28].

3.5. UV–Vis absorption spectra analysis: The UV–Vis absorption spectra of the as-prepared ZnO seeds, ZnO arrays and grassy ZnO are shown in Fig. 8*a*. All the samples show intrinsic absorption of ZnO in UV region. The grassy ZnO exhibits stronger absorption than ZnO seeds and ZnO arrays in UV–Vis region, indicating the absorption of more light energy and potential better photocatalytic properties. Usually, the energy bandgap (E_g) can be calculated using the formula as follows: $\alpha h\nu = A(h\nu - E_g)^{1/2}$, where α is an absorption coefficient, h is a Plank's constant, A is constant.

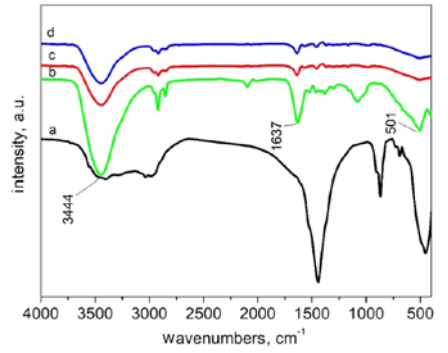

Fig. 7 *FTIR spectra of the samples*
a Seeds
b Grass-1
c Arrays
d Grass-2

doi: 10.1049/mnl.2020.0017

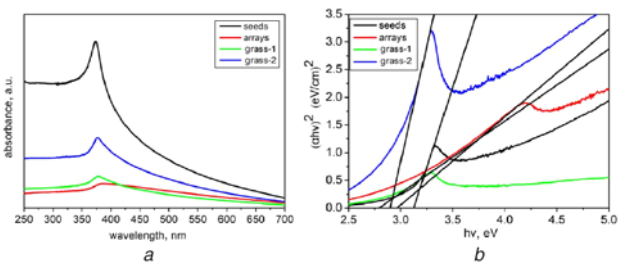

Fig. 8 *The optical properties of the samples*
a UV–Vis absorption spectra of the samples
b Tauc plots of the samples

Based on the formula, the tauc plots are determined from the UV–Vis spectra to investigate the bandgap energies of the samples. As can be shown in Fig. 8*b*, the bandgaps of the four samples (seeds, arrays, Grass-1 and Grass-2) are 3.2, 2.93, 2.79 and 2.89 eV, respectively. Obviously, the bandgaps of the ZnO array and grass are decreased compared with the seeds. The smaller the data, probably the better the photocatalytic performance [29, 30]. This conclusion is in good agreement with the photocatalytic properties.

3.6. Photocatalytic activity: The photocatalytic activity towards the photodecomposition of MB dyes of as-prepared ZnO with different latitude was displayed in Fig. 9*a*. Under ultraviolet light radiation, the efficiency of grassy ZnO to degrade the MB is greater than that of ZnO seeds and ZnO arrays. The degradation efficiency of grassy ZnO reaches ~90% after 150 min irradiation, which is much higher than that of ZnO seeds and ZnO arrays with only about 50%. This may be attributed to grassy ZnO with special needle structure, which is more favourable to accelerate the degradation of MB dye. The result is superior to that of ZnO film with different thickness [19].

In order to investigate the photocatalytic stability of the grassy ZnO for the degradation of MB solution, the periodic photodegradation experiment of ZnO Grass-1 was carried out. The performance is evaluated after five cycles for MB photodegradation under UV illumination as shown in Fig. 9*b*. With the rise of cycle index, the degradation efficiency of the sample is always kept at a relatively high state. After five cycles, the photocatalytic activity of Grass-1 still stays above 85%, indicating that the grassy ZnO is stable with a sensitive response to ultraviolet irradiation.

3.7. Photocurrent measurement: The photocurrent response curves of the photocatalysts under UV irradiation were shown in Fig. 10. When ultraviolet light is turned on, e^- in the valence band (VB) can be excited to the conduction band (CB) and form photocurrents and photocurrent reaches balance as the recombination of e^- and h^+ saturates [25]. It can be seen that the addition of UV light clearly presents current responses in the photocatalysts. Conversely, the current rapidly decreases when the UV light is turned off. This phenomenon indicates that most of the photoinduced e^- on the surface transfer to FTO to generate photocurrent [31].

Furthermore, Grass-1 appears the largest current response (90 μA) compared with ZnO seeds, ZnO arrays and Grass-2, demonstrating that the grassy ZnO could obviously increase the response and efficiency of the light to obtain improved photocatalytic performance.

3.8. Mechanism analysis: The photocatalytic mechanism of the sample for the photocatalytic reaction is demonstrated in Fig. 11. The photocatalyst is excited to generate the holes in the VB which is due to the transition of the photo-generated electrons

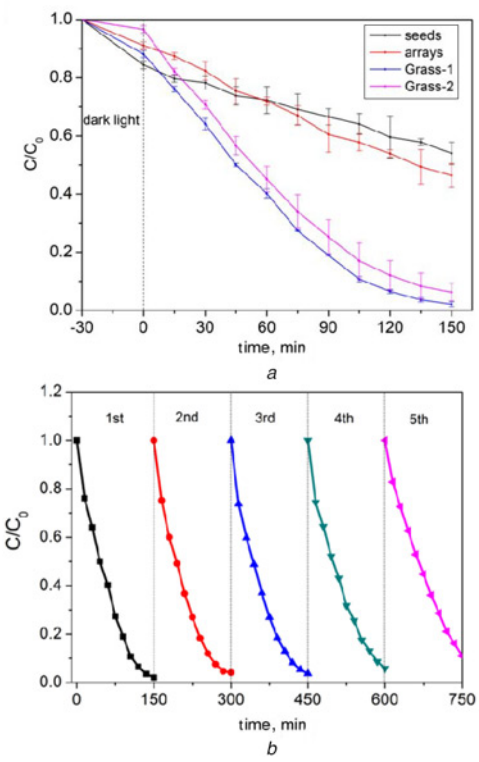

Fig. 9 *The photocatalytic properties of the samples*
a Photodegradation of MB solution using ZnO seeds, ZnO arrays and grassy ZnO nanostructure as photocatalysts under ultraviolet light
b Photodegradation of Grass-1 towards MB dyes for five cycles under illumination

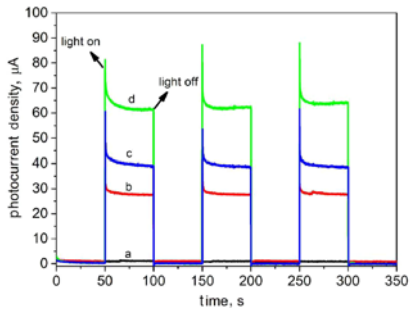

Fig. 10 *Photocurrent response of the samples*
a Seeds
b Arrays
c Grass-2
d Grass-1

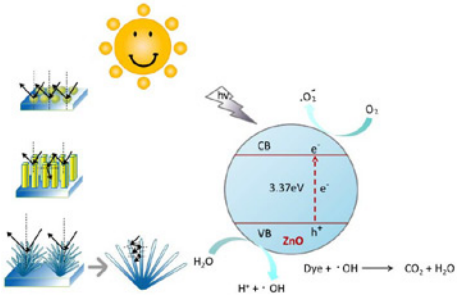

Fig. 11 *Schematic photocatalytic mechanism of the samples with different morphologies*

from VB to the CB under illumination [32]. The injected electrons prompt the conversion of oxygen molecule (O_2) to superoxide radical anion ($\cdot O_2^-$), which is the reduction reaction in order to eliminate MB molecules. Meanwhile, the holes boost the oxidation reaction between holes and H_2O for the production of active hydroxyl group (·OH). Herein, zinc oxide with different morphologies affects the reflection and absorption of the ultraviolet light. The UV light directly irradiates on the surfaces of the ZnO seeds and ZnO arrays. By comparison, grassy ZnO with thick zinc oxide needles forms multiple light reflections inside, which will greatly improve the light efficiency. The results show that the higher the light efficiency, the better the photocatalytic performance.

4. Conclusion: ZnO with different latitude morphologies were fabricated via an in situ growth on glass substrates by aqueous solution method. In the presence of the additive, the shape of the ZnO was changed from arrays to grass. The increased pH of the solution affected the aspect ratio of ZnO nanorods. The photocatalytic efficiency of grassy ZnO for the degradation of MB reached ∼90% and was superior to ZnO seed and ZnO array. The grassy ZnO with the largest photocurrent response also maintained relatively high performance after five cycles. Multiple light reflections inside grassy ZnO with thick needles greatly enhanced the light efficiency, resulting in good photocatalytic performance.

5. Acknowledgments: This work was financially supported by the National Natural Science Foundation of China (grant no. 61605027), the Program for New Century Excellent Talents in Fujian Province University (grant no. GY-Z18187) and the Fujian University of Technology Foundation (grant no. GY-Z15100).

6 References

[1] Francová A., Chrastný V., Šillerová H., *ET AL.*: 'Evaluating the suitability of different environmental samples for tracing atmospheric pollution in industrial areas', *Environ. Pollut.*, 2017, **220**, pp. 286–297
[2] Zhu X., Chen B., Zhu L., *ET AL.*: 'Effects and mechanisms of biochar-microbe interactions in soil improvement and pollution remediation: a review', *Environ. Pollut.*, 2017, **227**, pp. 98–115
[3] Wang Q., Yang Z.: 'Industrial water pollution, water environment treatment, and health risks in China', *Environ. Pollut.*, 2016, **218**, pp. 358–365
[4] Suwanboon S., Amornpitoksuk P., Randorn C.: 'Effect of tartaric acid as a structure-directing agent on different ZnO morphologies and their physical and photocatalytic properties', *Ceram. Int.*, 2019, **45**, pp. 2111–2116
[5] Zangeneh H., Zinatizadeh A.A.L., Habibi M., *ET AL.*: 'Photocatalytic oxidation of organic dyes and pollutants in wastewater using different modified titanium dioxides: A comparative review', *J. Ind. Eng. Chem.*, 2015, **26**, pp. 1–36
[6] Xiao X., Tu S., Lu M., *ET AL.*: 'Discussion on the reaction mechanism of the photocatalytic degradation of organic contaminants from a viewpoint of semiconductor photo-induced electrocatalysis', *Appl. Catal. B, Environ.*, 2016, **198**, pp. 124–132
[7] Calzada L.A., Castellanos R., García L.A., *ET AL.*: 'Tio_2, SnO_2 and ZnO catalysts supported on mesoporous SBA-15 versus unsupported nanopowders in photocatalytic degradation of methylene blue', *Microporous Mesoporous Mat.*, 2019, **285**, pp. 247–258
[8] You D., Xu C., Qin F., *ET AL.*: 'Interface control for pure ultraviolet electroluminescence from nano-ZnO-based heterojunction devices', *Sci. Bull.*, 2018, **63**, pp. 38–45
[9] Basahel S.N., Ali T.T., Mokhtar M., *ET AL.*: 'Influence of crystal structure of nanosized ZrO_2 on photocatalytic degradation of methyl orange', *Nanoscale Res. Lett.*, 2015, **10**, p. 73
[10] Ahmed B., Kumar S., Ojha A.K., *ET AL.*: 'Facile and controlled synthesis of aligned WO_3 nanorods and nanosheets as an efficient photocatalyst material', *Spectroc. Acta Pt. A-Molec. Biomolec. Spectr.*, 2017, **175**, pp. 250–261
[11] Sampaio M.J., Lima M.J., Baptista D.L., *ET AL.*: 'Ag-loaded ZnO materials for photocatalytic water treatment', *Chem. Eng. J.*, 2017, **318**, pp. 95–102
[12] Jiang H., Zhang X., Gu W., *ET AL.*: 'Synthesis of ZnO particles with multi-layer and biomorphic porous microstructures and ZnO/rGO composites and their applications for photocatalysis', *Chem. Phys. Lett.*, 2018, **711**, pp. 100–106
[13] Ahmed M.A.M., Mwankemwa B.S., Carleschi E., *ET AL.*: 'Effect of Sm doping ZnO nanorods on structural optical and electrical properties of Schottky diodes prepared by chemical bath deposition', *Mater. Sci. Semicond. Proc.*, 2018, **79**, pp. 53–60
[14] Atabaev T.S.: 'Size-dependent water splitting activity of ZnO nanorods', *Mater. Today Proc.*, 2019, **105**, pp. 15–18
[15] Haider A.J., Sultan F.I., Al-Nafiey A.: 'Controlled growth of different shapes for ZnO by hydrothermal technique'. AIP Conf. Proc., Beirut, Lebanon, 2018, vol. 1, p. 030085
[16] Liu L., Liu Z., Yang Y., *ET AL.*: 'Photocatalytic properties of Fe-doped ZnO electrospun nanofibers', *Ceram. Int.*, 2018, **44**, pp. 19998–20005
[17] Li X., Liu D., Zhu B., *ET AL.*: 'Facile preparation of ZnO/Ag_2CO_3 heterostructured nanorod arrays with improved photocatalytic activity', *J. Phys. Chem. Solids*, 2019, **125**, pp. 96–102
[18] Wu X., Wen L., Lv K., *ET AL.*: 'Fabrication of ZnO/graphene flake-like photocatalyst with enhanced photoreactivity', *Appl. Surf. Sci.*, 2015, **358**, pp. 130–136
[19] Mauro A.D., Fragala M.E., Privitera V., *ET AL.*: 'Zno for application in photocatalysis: from thin films to nanostructures', *Mater. Sci. Semicond. Proc.*, 2017, **69**, pp. 44–51
[20] Hariharan C.: 'Photocatalytic degradation of organic contaminants in water by ZnO nanoparticles: revisited', *Appl. Catal., A*, 2006, **304**, pp. 55–61
[21] Ye X.X., Wang Z.P., Li Z.D., *ET AL.*: 'Zno nanorod array/reduced graphene oxide substrate with enhanced performance in photocatalytic degradation', *Micro. Nano. Lett.*, 2019, **14**, pp. 868–871
[22] Tian J.H., Hu J., Li S.S., *ET AL.*: 'Improved seedless hydrothermal synthesis of dense and ultralong ZnO nanowires', *Nanotechnology*, 2011, **22**, p. 245601
[23] Thongam D.D., Gupta J., Sahu N.K., *ET AL.*: 'Investigating the role of different reducing agents, molar ratios, and synthesis medium over the formation of ZnO nanostructures and their photo-catalytic activity', *J. Mater. Sci.*, 2018, **53**, pp. 1110–1122
[24] Chu D., Masuda Y., Ohji T., *ET AL.*: 'Facile synthesis, characterization of ZnO nanotubes and nanoflowers in an aqueous solution', *J. Am. Ceram. Soc.*, 2010, **93**, pp. 887–893
[25] Han Z.Z., Liao L., Wu Y.T., *ET AL.*: 'Synthesis and photocatalytic application of oriented hierarchical ZnO flower-rod architectures', *J. Hazard. Mater.*, 2012, **217–218**, pp. 100–106
[26] Mohajerani M.S., Mazloumi M., Lak A., *ET AL.*: 'Self-assembled zinc oxide nanostructures via a rapid microwave-assisted route', *J. Cryst. Growth*, 2008, **310**, pp. 3621–3625
[27] Manikandan A., Manikandan E., Meenatchi B., *ET AL.*: 'Rare earth element (REE) lanthanum doped zinc oxide (La: ZnO) nanomaterials: synthesis structural optical and antibacterial studies', *J. Alloy Compd.*, 2017, **723**, pp. 1155–1161
[28] Moghaddam E., Youzbashi A.A., Kazemzadeh A., *ET AL.*: 'Preparation of surface-modified ZnO quantum dots through an ultrasound assisted sol–gel process', *Appl. Surf. Sci.*, 2015, **346**, pp. 111–114
[29] El-Yazeed W.A., Ahmed A.I.: 'Photocatalytic activity of mesoporous WO_3/TiO_2 nanocomposites for the photodegradation of methylene blue', *Inorg. Chem. Commun.*, 2019, **105**, pp. 102–111
[30] Selvin S.S.P., Radhika N., Borang O., *ET AL.*: 'Visible light driven photodegradation of rhodamine B using cysteine capped Zno/GO nanocomposite as photocatalyst', *J. Mater. Sci., Mater. Electron.*, 2017, **28**, pp. 6722–6730
[31] Han Z.Z., Ren L., Cui Z., *ET AL.*: 'Ag/ZnO flower heterostructures as a visible-light driven photocatalyst via surface plasmon resonance', *Appl. Catal. B, Environ.*, 2012, **126**, pp. 298–305
[32] Fan J., Li T., Heng H.: 'Hydrothermal growth of ZnO nanoflowers and their photocatalyst application', *Bull. Mat. Sci.*, 2016, **39**, pp. 19–26

doi: 10.1049/mnl.2020.0017